Computer Assisted Mechanics and Engineering Sciences, 11: 99–118, 2004.
Copyright © 2004 by Institute of Fundamental Technological Research, Polish Academy of Sciences

Combined shape and non-shape sensitivity for optimal design of metal forming operations

Horacio J. Antúnez, Maciej Kowalczyk
Institute of Fundamental Technological Research
Polish Academy of Sciences, Świetokrzyska 21, 00-049 Warsaw, Poland
e-mail: hantunez@ippt.gov.pl, mkowal@ippt.gov.pl

(Received October 29, 2002)

Shape and non-shape optimization is carried out for metal forming processes. This means a unified treatment of both shape parameters and other process parameters which are assumed to be design variables. An optimization algorithm makes use of the results of the analysis problem and of the sensitivity parameters obtained as a byproduct of the basic solution, in the context of the direct differentiation method. The shape sensitivity stage is formulated within the domain parametrization approach. Two alternative mappings are proposed to obtain the required derivatives with respect to the shape parameters. The behaviour of different functionals considered and the effect of the boundary conditions on the optimal design are discussed.

1. Introductory comments

For many years, optimization and numerical simulation of engineering problems were two independent disciplines. As it is well known, the potential of analysis offered by numerical simulation techniques drew design tasks into a new era. Research effort was then largely devoted to produce reliable tools for analysis, which in turn involved several scientific areas. But still the optimal design was for long time searched for by trial and error, making good use of the engineer's experience and intuition. A real hint towards a more automatized optimization appeared with the development of the so-called analytical methods for sensitivity analysis, from which the derivatives of given functionals involving the problem variables were available at a relatively low computational cost, as a byproduct of the solution of the analysis problem. The way for gradient-based optimization was, then, open.

Indeed, even if it is true that non-gradient-based optimization procedures are sometimes used, it is also obvious that their applicability is largely limited by the cost of each functional evaluation. When such functional evaluation involves the solution by finite elements of a nonlinear problem, such methods may be simply discouraging. Their lack of effectiveness is very clearly seen here in comparison with their gradient-based counterpart. For this reason shape optimization was practically not undertaken until the concept of sensitivity analysis – in particular to shape parameters – , became more popular. Some attempts were carried out when the repetitive solution of engineering problems within an acceptable accuracy began to be affordable. The first works on optimization combined with numerical modelling concern mainly structural analysis [1, 2] and thermal problems [3]. In the field of metal forming, one of the first works can be found in [4, 5], where both non-gradient and gradient-based optimization was performed, the latter using finite differences (FDM) to calculate the numerical derivatives. In a similar context, that is, without using analytical shape sensitivity, optimal design of forging die shapes was presented in [6], which obviously involves a higher degree of complexity due to the transient nature of this process.

The importance of these results is out of discussion. If numerical simulation means a dramatic reduction in the number of necessary prototypes, now the use of optimization algorithms may lead

to a sensible reduction in the number of necessary numerical simulations in order to obtain the optimal design. In addition, it provides a rigorous methodology to perform this task. A certain degree of automation and generality is required if the procedure aims to have practical applications. Besides, for such tool to be effective a series of conditions must still be fulfilled. First, the numerical model must reflect the key features of the process. Second, a complete sensitivity analysis must be carried out, which requires a proper description of the discretized domain in terms of (as few as possible) design parameters, and this in turn implies the definition of the functions by which the nodal coordinates depend on those design parameters. Next, the design functional and its gradient in the design space must be evaluated. The optimization algorithm will make use of these quantities to find a new trial for the optimal shape until the functional is minimized subject to some necessary design constraints which limit the trials of design sets. Let us notice that the proper definition of the design criterion and constraints still requires the advice of an expert. But now different functionals may be easily tested and minimized, compared their respective optima and their values and their behaviour at the optima of other functionals.

The lack of some of the above mentioned elements will probably deteriorate the performance of the optimization procedure. For this reason it is crucial to have a complete and consistent treatment of the whole problem. However, the idea of optimization is not new and does not involve special theoretical difficulties. Instead, once the analysis and the sensitivity stages are available, its application to optimization is straightforward. But the main difficulty may have been to achieve those tools. In the last years some works concerning shape optimization of metal forming processes have been presented, assuming the usage of advanced techniques for sensitivity analysis. In [7] the shape optimization of a 3D extrusion die is presented. Even if the tangent matrix is used to evaluate the sensitivity coefficients, the explicit derivatives with respect to the design variables are calculated by FDM, using the so-called 'discrete semi-analytical direct differentiation approach to sensitivity evaluation'. The authors analyze the effect of the perturbation size which, as expected, deserves special attention. In the reported work, after analyzing perturbations ranging from 10^{-2} to 10^{-12}, an area was found were apparently similar results are obtained for either backward, centered and forward differences. However, the optimum size of the perturbation seems to be different for each design variable. This fact further complicates the problem, and supports the use of analytical evaluation of the explicit derivatives, using one of the available approaches, e.g. domain parameterization (DPA) [8–10], material derivative (MDA) [11, 12], etc. Moreover, it is clear that the FDM implies more calculation time and results in an awkward code as compared with the analytical version. Concerning again forging, matrix shape optimization was presented in [13–15], and more recently in [16–18]. Other recent works have also considered a more elaborate (e.g. elastoplastic) material model or motion description [19–22] or by alternative analysis methods [23]. Again the merits of such approaches are evident, even if they did not get rid of finite difference-based explicit derivatives. Let us add that up to now, very rarely a full analytical sensitivity based optimization (i.e. without any FDM approximation) has been carried out. Among such works, preform and die design shapes have been optimized in [24] and [25], respectively.

In this paper, some results concerning optimization within extrusion processes are shown. They are based on previous work [8, 26–29, 36] concerning sensitivity analysis to different parameters of a given problem such as material properties, friction coefficients, ram velocity, etc. (i.e. non-shape variables), and to other parameters used to define the problem geometry (i.e. shape variables). A brief outline of the formalism is given (Sec. 2). The above distinction on the design variables justifies the expression "shape and non-shape" sensitivity [30], sometimes used. In a rather abstract context both kind of variables allow a unified treatment. However, specific implementations give rise to their own terms which make clear the need of a separate treatment for them. In particular, shape sensitivity requires further assumptions to express the derivatives of every geometric quantity of the problem in terms of the shape parameters. In other words, a mapping scheme is needed to establish the required dependence between them. Two such mappings are presented in Sec. 2.3. Special attention should be paid to what we called bispline mapping, which allows for the use of angles as design variables, which, combined with the traditional set of spacial coordinates,

improves the efficiency of solution. After this, the optimization procedure is schematized and finally illustrated by carrying out the shape optimization of a die for direct extrusion and the simultaneous optimization of shape and non-shape variables within a combined direct-inverse extrusion process. Two available optimization procedures [31, 32] are used to this purpose. The performance of both proposed methods for mapping is shown. Some remarks are made, concerning the behaviour of the investigated functionals and the effect on the optimal shape of boundary conditions, as it came out along the numerical illustrations.

2. Numerical model and sensitivity analysis

2.1. Outline of the flow approach

The flow of metal under forming conditions is described by the equilibrium equation in rate-form, where usually convective (i.e. dynamic) terms are neglected

$$\int_{\Omega} \boldsymbol{\sigma} \cdot \delta\dot{\boldsymbol{\varepsilon}} \, \mathrm{d}\Omega = \int_{\Omega} \mathbf{f} \, \delta\mathbf{v} \, \mathrm{d}\Omega + \int_{\partial\Omega_\sigma} \mathbf{t} \, \delta\mathbf{v} \, \mathrm{d}(\partial\Omega) \,. \tag{1}$$

A fluid-type constitutive equation of a non-Newtonian kind is assumed

$$\sigma_{ij} = \sigma^{\mathrm{D}}_{ij} - p\,\delta_{ij} = 2\mu\,\dot{\varepsilon}_{ij} - p\,\delta_{ij} \tag{2}$$

where

$$\mu = \frac{1}{3\dot{\bar{\varepsilon}}} \left[\sigma_0 + \left(\frac{\dot{\bar{\varepsilon}}}{\gamma} \right)^{\frac{1}{n}} \right] \tag{3}$$

with the incompressibility condition additionally imposed. After discretization, the above system yields, in residual form

$$\mathbf{R} = \mathbf{K}^{(S)}\overline{\mathbf{q}} - \overline{\mathbf{Q}} = \begin{bmatrix} \mathbf{K}_{(\mu)} & \mathbf{K}^{\mathrm{T}}_{(\mathrm{p})} \\ \mathbf{K}_{(\mathrm{p})} & \mathbf{0} \end{bmatrix} \begin{bmatrix} \dot{\mathbf{q}} \\ \overline{\mathbf{p}} \end{bmatrix} - \begin{bmatrix} \mathbf{Q} \\ \mathbf{0} \end{bmatrix} = \mathbf{0} \tag{4}$$

where

$$\begin{aligned} \mathbf{K}_{(\mu)} &= \int_{\Omega} \mu\,\mathbf{k}_0 \, \mathrm{d}\Omega = \int_{\Omega} 2\mu\,\mathbf{B}^{\mathrm{T}}\,\mathbf{B} \, \mathrm{d}\Omega \,, \\ \mathbf{K}^{\mathrm{T}}_{(\mathrm{p})} &= -\int_{\Omega} \mathbf{k}^{\mathrm{T}}_{(\mathrm{p})} \, \mathrm{d}\Omega = -\int_{\Omega} \mathbf{B}^{\mathrm{T}} \boldsymbol{\Gamma}\, \widehat{\mathbf{B}} \, \mathrm{d}\Omega \,, \\ \mathbf{Q} &= \int_{\Omega} \boldsymbol{\phi}\widehat{\mathbf{f}} \, \mathrm{d}\Omega + \int_{\partial\Omega_\sigma} \boldsymbol{\phi}\widehat{\mathbf{t}} \, \mathrm{d}(\partial\Omega) + \mathbf{P} \,, \end{aligned} \tag{5}$$

while $\dot{\mathbf{q}}$ and $\overline{\mathbf{p}}$ are, respectively, the discretized velocity and pressure vectors, $\boldsymbol{\phi}$ the array of shape functions for velocity, $\mathbf{B}$ the standard strain rate-velocity matrix and $\mathbf{P}$ the vector of concentrated loads applied at the nodes. $\widehat{\mathbf{B}}$ (analogous to $\mathbf{B}$) coincides with the array of shape functions for pressure, and the column vector $\boldsymbol{\Gamma}$ converts the total strain into its volumetric components.

Out from Eq. (4), the tangent matrix is obtained as

$$\frac{\partial \mathbf{R}}{\partial \overline{\mathbf{q}}} = \mathbf{K}^{(S)} + \int_{\Omega} (\overline{\mathbf{k}}_0 \overline{\mathbf{q}}) \frac{\partial \mu}{\partial \overline{\mathbf{q}}} \, \mathrm{d}\Omega - \frac{\partial \overline{\mathbf{Q}}}{\partial \overline{\mathbf{q}}} = \mathbf{K}^{(T)} \tag{6}$$

$\left(\text{where } \overline{\mathbf{k}}_0 = \begin{bmatrix} \overline{\mathbf{k}} & 0 \\ 0 & 0 \end{bmatrix} \right)$, which is used for Newton–Raphson solution of Eq. (4) and for the sensitivity stage.

2.2. Material parameter sensitivity (DDM)

Without going into further details already discussed (e.g. [28]), calculation of the sensitivity of a given functional to a design parameter h requires (in terms of the direct differentiation method, DDM) the sensitivity of the problem unknowns, i.e. $\mathrm{d}\overline{\mathbf{q}}/\mathrm{d}h$, which results from differentiating Eq. (4) with respect to the design parameter h. Since the vector $\overline{\mathbf{q}}$ has been solved for from the equilibrium problem, we have

$$\mathbf{K}^{(T)}\frac{\mathrm{d}\overline{\mathbf{q}}}{\mathrm{d}h} = -\left(\int_{\Omega}\frac{\partial\mu}{\partial h}\overline{\mathbf{k}}_0\,\mathrm{d}\Omega\right)\overline{\mathbf{q}} + \frac{\partial\overline{\mathbf{Q}}}{\partial h} \tag{7}$$

whenever h is a design parameter not involved in the shape description. But if, instead, h is a shape parameter, a number of new terms appear from the differentiation of the particular quantities appearing in Eq. (4). All of them may be routinely computed from the already defined model, provided a law relating coordinates of a generic point to the design parameters is established. This is discussed in the next subsection, 2.3.

2.3. Mapping for shape sensitivity (DPA)

To define such dependence, sometimes a problem dependent parameterization has been preferred, e.g. [7]. Here, instead, a more flexible approach is searched for, as used in [8–10, 33, 34]. It consists in a new discretization, usually much coarser than the one used to solve the equilibrium problem. The only condition required from it is an accurate description of the domain. We have thus design nodes, which are connected by design elements. Now a given mapping is specified once these design elements are defined. After that, we will be able to calculate the derivatives $\partial x_i/\partial X_j^{\alpha}$, where X_j^{α} is the j-th coordinate of the design node α, with $\alpha = 1, ..., N_{DN}$, where N_{DN} is the number of design nodes. This derivative is required to differentiate each of the quantities of Eq. (4) by application of the chain rule. Within this formalism, a generic scalar quantity a, for example, is differentiated as

$$\frac{\partial a}{\partial h} = \frac{\partial a}{\partial x_i}\frac{\partial x_i}{\partial X_j^{\alpha}}\frac{\partial X_j^{\alpha}}{\partial h}, \quad \alpha = 1, ..., N_{DN}, \quad i, j = 1, 2 \tag{8}$$

where X_j^{α} is the j-th coordinate of the α-th design node and x_i are the spatial coordinates. Expressions for other quantities (vectors, tensors, differential operators, etc.) are developed as well ([8, 11, 28, 33]). Equation (8) and analogous expressions for other quantities present the explicit derivatives with respect to the design variables and thus will be grouped on the right-hand side of Eq. (7). However, the total derivatives with respect to the design variables may also include terms that are implicitly dependent on design, i.e. through the sensitivities. But these terms, by definition of the tangent stiffness matrix, enter the left-hand side of Eq. (7).

The following mapping schemes are thought of for 2D. Nevertheless, their extension to 3D is straightforward.

2.3.1. Bilinear design elements

We first consider bilinear elements, using the known shape functions used in finite elements, or a similar procedure to obtain the local (i.e. within the design elements) coordinates of the points laying inside the element. We can thus obtain the derivatives $\partial x_i/\partial X_j^{\alpha}$, as is usually done within isoparametric elements. Then, assuming that our design variables are some of the design-node coordinates, $h = X_{\underline{j}}^{\underline{\alpha}}$, we have $\partial X_j^{\alpha}/\partial h = \delta_{\alpha\underline{\alpha}}\delta_{j\underline{j}}$. Both quantities are then replaced in expressions like Eq. (8) or similar.

2.3.2. Domain parameterization with bispline design elements

Within bilinear elements, the boundary of the discretized domain is described by linear interpolation between design nodes. Aiming at a more elaborate boundary description, the design-discretization is now considered in two steps (this procedure is similar to that considered in [3]).

1) *Spline interpolation of the contour subject to design.* The boundary of the discretized domain must be described as a combination of straight lines and some higher order curves. To define each of them, the coordinates and possibly the angle with respect to a selected coordinate axis of a set of nodes is used. For such purpose cubic splines (which may be reduced trivially to a straight line segment) are very commonly used and defined by an appropriate set of nodal coordinates and angles with respect to a reference direction. These nodal coordinates and angles are thus the (natural) design variables. However, it may be sometimes useful to take the spline coefficients instead.

2) *Double-spline-interpolated 4×4-node design elements,* in terms of which it is possible to find the derivative of the coordinates of any point (finite element discretization node) with respect to the nodal coordinates of the design element. It should be noticed that these nodal coordinates of the design element may not be independent. In fact, in order to get a smooth field of local coordinates the nodes which do not define a border may be calculated as linearly interpolated from the corner nodes.

The procedure is similar to that considered in [3]) and it is used to construct bispline design elements (by bispline we mean a two-variable function resulting as the product of two one-variable spline functions).

1) Spline interpolation of the boundary subject to design

The basic shape optimization problem may be formulated as that of obtaining the shape that minimizes a given cost functional. For different reasons, not all the boundary may be subject to optimization: most frequently some design constrains have to be met. On the other hand, we have the problem of choosing the geometric variables that can describe the boundary upon design. In principle, it is not a good choice to use as design variables the coordinates of each of the boundary nodes arising from the finite element discretization. It is well known that optimization algorithms may become very slow and even have convergence problems for a large number of design variables. Moreover, such a large number may be not necessary if, additionally, the nodes on the border subject to optimal design are interpolated with sufficiently smooth functions which, in turn, are defined in terms of a few master nodes.

Any cubic spline segment involves the evaluation of four coefficients resulting from the fulfillment by the function of four conditions on its value or its derivatives at given points. Let us divide (part of) a boundary to be optimized into a number of segments, and let us define a spline in each of them. Neighbouring segments must satisfy the continuity condition of the curve and of its first derivative. As a required additional assumption to find the optimal shape, the design nodes and, thus, all the other nodes laying in between may be allowed to move according to a specified direction, typically holding one of the spatial coordinates fixed, i.e. making them depend linearly on the internal spline variable. So, the other spatial coordinates of the design nodes and the slope of the boundary on them with respect to a reference direction constitute the design variables and both are functions of the spline internal variable. Within such parameterization technique, the conditions between segments are easily assured and the addition of more segments to describe the boundary under design is automatized. Hence, when the boundary under design is described with only one spline segment, four design variables appear (some of which may be fixed by a design constraint). However, for every new added segment, although four more parameters enter, only two more design variables are added, because of the continuity conditions between spline segments. In addition, this set of variables allows us to find out the spline coefficients separately for each segment.

For a generic segment k we have thus a vector of design variables

$$\mathbf{h}^k = \left\{ \widehat{X}_i^k, \widehat{X}_i'^k, \widehat{X}_i^{k+1}, \widehat{X}_i'^{k+1} \right\} \tag{9}$$

where $\widehat{X}_i^k, \widehat{X}_i^{k+1}$ are the (variable) coordinates of the end-of-spline-segment design nodes and the primed quantities mean derivatives with respect to the spline variable. The slope of the design contour and, further, its angle with respect to a reference axis will be associated to them. We find the coefficients of the spline

$$\chi(\xi) = e_0 + e_1\xi + e_2\xi^2 + e_3\xi^3\,; \qquad -1 \le \xi \le 1 \tag{10}$$

by requiring that

$$\widehat{X}_i^k = \chi(-1)\,; \quad \widehat{X}_i'^k = \chi'(-1)\,; \quad \widehat{X}_i^{k+1} = \chi(1)\,; \quad \widehat{X}_i'^{k+1} = \chi'(1) \tag{11}$$

2) Interpolation inside the design element

In terms of the internal coordinates ξ, η we define the double spline functions, for $i = 1, 2$

$$\begin{aligned}\Psi_i = {} & a_1^i + a_2^i\xi + a_3^i\eta + a_4^i\xi^2 + a_5^i\xi\eta + a_6^i\eta^2 + a_7^i\xi^3 + a_8^i\xi^2\eta + a_9^i\xi\eta^2 + a_{10}^i\eta^3 \\ & + a_{11}^i\xi^3\eta + a_{12}^i\xi^2\eta^2 + a_{13}^i\xi\eta^3 + a_{14}^i\xi^3\eta^2 + a_{15}^i\xi^2\eta^3 + a_{16}^i\xi^3\eta^3\end{aligned} \tag{12}$$

where $-1 \le \xi, \eta \le 1$, and the sixteen coefficients of each function are determined by the nodal coordinates at $\xi, \eta = \left\{ -1, -\frac{1}{3}, \frac{1}{3}, 1 \right\}$. For practical purposes the nodal coordinates may be mutually independent or, better, those which are unnecessary to describe the geometry may be calculated in terms of the other nodes. In this case the local coordinate field will be smoother and the finite element mesh will conserve its regular aspect.

The whole shape that is being optimized may be piece-wise described by spline lines, as seen above. Each of these spline segments may correspond to one side of the design elements in which the whole domain can be subdivided. Then, the number of design elements is roughly determined by the number of segments needed to define the geometry with a given accuracy (plus a few more elements for those areas not subject to design). Most frequently, only one side (or none) of the design element will be a spline segment. The remaining three sides can be straight lines. In such an element we have to define the above Ψ_i functions in order to relate the coordinates of each point contained in the element with the design variables via the nodal coordinates of the design element and the spline coefficients of the design-boundary segment corresponding to the design element. Having defined this mapping, the way the nodes change their position with design variations is uniquely determined, and we can calculate the derivatives $\mathrm{d}x_i/\mathrm{d}h_d$, which are needed to obtain the global sensitivity coefficients and, with them, the gradient of the objective function.

To specifically obtain these derivatives we proceed design-element-wise as follows:

1) Define a spline for the design element side subject to design in terms of the design variables connected by the design element, as shown above. The other coordinate (y in this case) is linearly interpolated within the internal variable ξ and does not enter the design variables. The other three sides of the design element are straight lines.

2) Define a double-spline in the design element. We need a set of sixteen points (x and y coordinates) from which we obtain two sets of sixteen constants. We take as reference points those located at $(\xi, \eta) = \left\{ -1, -\frac{1}{3}, \frac{1}{3}, 1 \right\}$ (Fig. 1). Points 1, 4, 13 and 16 are known. We obtain points 2, 3, 5, 8, 9 and 12 as linearly interpolated from the corner nodes. Points 14 and 15 are obtained by evaluating χ at $\xi = -\frac{1}{3}$ and $\xi = \frac{1}{3}$ respectively, and finally, points 6 and 10, and 7 and 11, by linear interpolation on the η direction between points 2 and 14, and 3 and 15 respectively.

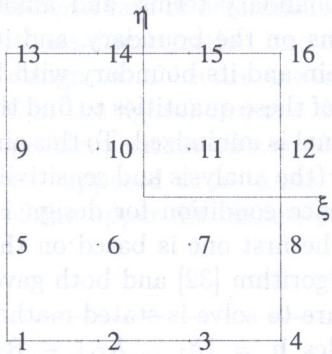

Fig. 1. Design element

If we arrange the local coordinates and the interpolating functions in the vectors (see Fig. 1)

$$\boldsymbol{\xi} = \left\{-1, -\frac{1}{3}, \frac{1}{3}, 1, -1, -\frac{1}{3}, \frac{1}{3}, 1, -1, -\frac{1}{3}, \frac{1}{3}, 1, -1, -\frac{1}{3}, \frac{1}{3}, 1\right\} \tag{13}$$

$$\boldsymbol{\eta} = \left\{-1, -1, -1, -1, -\frac{1}{3}, -\frac{1}{3}, -\frac{1}{3}, -\frac{1}{3}, \frac{1}{3}, \frac{1}{3}, \frac{1}{3}, \frac{1}{3}, 1, 1, 1, 1\right\} \tag{14}$$

$$\boldsymbol{\psi} = \left\{1, \xi, \eta, \xi^2, \xi\eta, \eta^2, \xi^3, \xi^2\eta, \xi\eta^2, \eta^3, \xi^3\eta, \xi^2\eta^2, \xi\eta^3, \xi^3\eta^2, \xi^2\eta^3, \xi^3\eta^3\right\} \tag{15}$$

we can rewrite the double splines as

$$\Psi_i = a_r^i \psi_r\,, \qquad r = 1, ..., 16\,, \qquad i = 1, 2\,. \tag{16}$$

Arranging accordingly the global coordinates in vectors $\widetilde{\mathbf{X}}_i$ by evaluating the functions ψ_r at the points (ξ_s, η_s) we have

$$\widetilde{X}_{is} = c_{sr} a_r^i\,, \qquad r, s = 1, ..., 16\,, \qquad i = 1, 2 \tag{17}$$

with $c_{sr} = \psi_r(\xi_s, \eta_s)$, from which

$$a_r^i = (c_{rs})^{-1} \widetilde{X}_{is}\,, \qquad r, s = 1, ..., 16\,, \qquad i = 1, 2\,. \tag{18}$$

Now we can calculate the derivative

$$\frac{\partial x_i}{\partial h_d} = \frac{\partial x_i}{\partial a_r^i} \frac{\partial a_r^i}{\partial \widetilde{X}_s^i} \frac{\partial \widetilde{X}_s^i}{\partial \chi} \frac{\partial \chi}{\partial e_m} \frac{\partial e_m}{\partial h_d}\,, \qquad \begin{array}{ll} r, s = 1, ..., 16 & \text{no sum on } i = 1, 2 \\ m = 0, ..., 3 & d = 1, ..., D \end{array} \tag{19}$$

where $\partial a_j / \partial \widetilde{X}_k = (c^{-1})_{jk}$. We may notice that the derivative $\mathrm{d}\widetilde{X}_s^i / \mathrm{d}\chi = 0$ for those i not used in the definition of χ, Eqs. (9) to (11).

It is worth to point out that for elements having all four sides straight, the above mapping reduces to the bilinear one referred to in Sec. 2.3.1.

3. Optimization algorithm

Having a reliable numerical simulation of the problem at hand and of its sensitivity to a set of design parameters, the optimization problem can be faced. The previously obtained results are used to evaluate a given response functional

$$\mathcal{G} = \int_0^t \left[\int_{\Omega(\mathbf{h})} G(\boldsymbol{\sigma}^{\mathrm{D}}, \overline{\mathbf{q}}; \mathbf{h})\, \mathrm{d}\Omega + \int_{\partial\Omega_v(\mathbf{h})} g(\overline{\mathbf{q}}_F, \mathbf{t}; \mathbf{h})\, \mathrm{d}(\partial\Omega_v) + \int_{\partial\Omega_\sigma(\mathbf{h})} h(\overline{\mathbf{q}}, \mathbf{t}_F, \mathbf{h})\, \mathrm{d}(\partial\Omega_\sigma) \right] \mathrm{d}\tau \tag{20}$$

which may involve volume and boundary terms, and among the latter, those corresponding to imposed either velocity or tractions on the boundary, and its gradient in the design space. $\Omega(\mathbf{h})$, $\partial\Omega_v(\mathbf{h})$, $\partial\Omega_\sigma(\mathbf{h})$, denote the domain and its boundary with both types of imposed conditions. The optimization algorithm makes use of these quantities to find the optimal set of design parameters, i.e. that for which the response functional is minimized. To this aim, the problem is sequentially solved at each trial set of design parameters (the analysis and sensitivity module is called by the optimization procedure) until a given convergence condition for design is met. In this work, two optimization algorithms have been employed: the first one is based on the conjugate gradient method [31] and the second is the Schittkowski's algorithm [32] and both gave the same results.

The optimization problem we are to solve is stated mathematically as follows:
Find the vector of design variables $\mathbf{h} = \{h_1, ..., h_D\} \in \mathrm{R}^D$ that minimizes the objective functional (20) subject to

$$\begin{array}{ll} \Upsilon_a(\boldsymbol{\sigma}^{\mathrm{D}}, \overline{\mathbf{q}}; \mathbf{h}) = 0 & a = 1, ..., A\,, \\ \Upsilon_b(\boldsymbol{\sigma}^{\mathrm{D}}, \overline{\mathbf{q}}; \mathbf{h}) \leq 0 & b = 1, ..., B\,, \\ h_d^- \leq h_d \leq h_d^+ & d = 1, ..., D\,, \\ \text{Equilibrium equations} & \end{array} \tag{21}$$

where h_d^-, h_d^+ are lower and upper bounds imposed on the design basis h_d, $d = 1, 2, ..., D$. Objective and constraint (referred to as performance) functionals in the above optimization formulation call for design sensitivity analysis.

The optimization algorithm can be summarized as follows:

0. initial estimate for $\mathbf{h}$,
1. evaluation of $\mathcal{G}$ and $\dfrac{\mathrm{d}\mathcal{G}}{\mathrm{d}\mathbf{h}}$,
2. if $\left\| \dfrac{\mathrm{d}\mathcal{G}}{\mathrm{d}\mathbf{h}} \right\| \leq tol$ exit,
3. calculation of $\Delta\mathbf{h}$,
4. update $\mathbf{h}$: $\mathbf{h}^{(\mathrm{new})} = \mathbf{h}^{(\mathrm{old})} + \Delta\mathbf{h}$,
5. go to 1.

The set of design variables need not to have the same units. We have seen in Sec. 2.3.2 that some of the shape variables may be angles. Moreover, we can include some material parameters such as the yield stress, as it will be shown in Sec. 4.2, or even of another kind like ram velocity, friction coefficient, etc.

4. Computational illustrations

The model for optimization presented here has been tested on direct and direct-inverse extrusion problems. Several examples in which shape and non-shape variables were used to minimize different functionals – some of the obtained results are discussed below. First, optimization regarding only shape variables is considered, to better show the performance of the bispline design elements. Afterwards, combined shape and non-shape optimization is considered. Two non-shape variables are analized (i.e. yield stress and the ratio of direct and inverse flows), mainly to test the algorithm. Both types of variables – shape and non shape – thus enter together in the optimization procedure. Results agree with intuitive expectations, and show besides that, regarding the non-shape variables analized, shape variables are more important to reduce the cost functional.

4.1. Direct extrusion – shape optimization

The shape optimization procedure is first illustrated by finding the optimal design of a direct extrusion matrix, where the extrusion ratio is fixed. Optimization criteria of minimizing the deformation

energy, the maximum strain rate and uniform rate of deformation are investigated. A layout of the problem is shown in Fig. 2, together with its discretization into finite elements. A constant velocity is imposed on the left boundary. The design variables are the x coordinates of some nodal points defining the matrix shape (marked A-E in the figure) and the slope on the die boundary at them. The shape sensitivity analysis of such problem within bilinear design elements has been presented in [8]. In that paper the die profile was supposed to be a straight line, so that only one design parameter (the horizontal coordinate of the upper die corner, point A in Fig. 2) was sufficient to define any geometry variation.

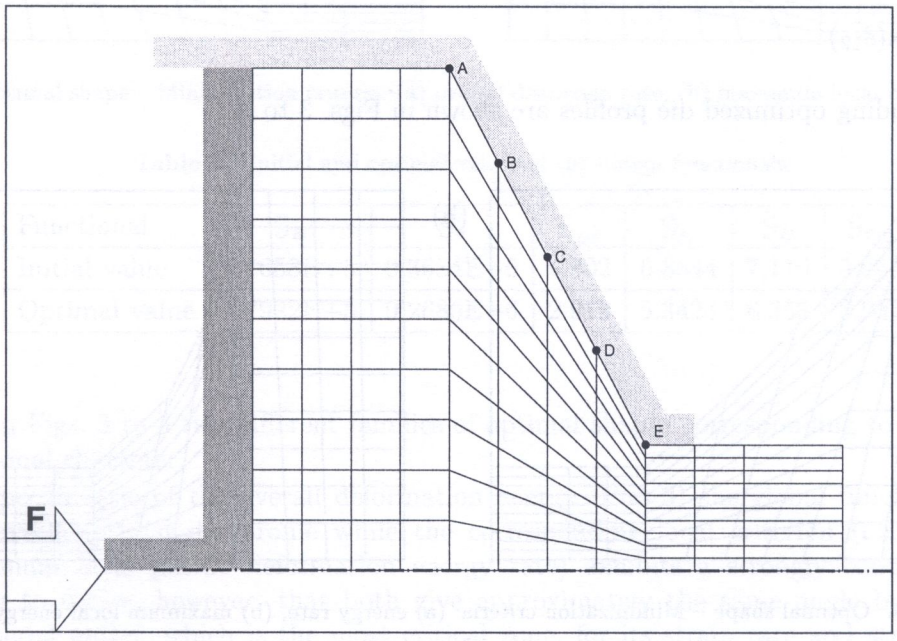

Fig. 2. Layout of the extrusion process

Using the flow approach we obtain the velocity, strain and stress solution. Further, for any given configuration the shape sensitivities may be obtained by application of the procedure presented in Sec. 2 for appropriately defined shape parameters.

On this basis, optimum shapes resulting from different design functionals and obtained using the bilinear design elements are first shown. Then, taking one design functional, the effect of friction boundary conditions on the optimum shape is analyzed. Finally, optimum shapes are obtained with different number of design variables using both bilinear and bispline design elements.

4.1.1. Design functionals

The following functionals have been employed:
energy rate

$$\mathcal{G}_E = \int_\Omega \sigma_{ij}\dot{\varepsilon}_{ij}\,\mathrm{d}\Omega\,, \tag{22}$$

maximum local energy rate

$$\mathcal{G}_e = \max_\Omega \left(\tfrac{1}{2}\sigma_{ij}\dot{\varepsilon}_{ij}\right)\,, \tag{23}$$

averaged effective strain rate deviation

$$\mathcal{G}_{D\dot{\bar{\varepsilon}}} = \frac{1}{\Omega}\int_\Omega \left(\dot{\bar{\varepsilon}} - \dot{\bar{\varepsilon}}^*\right)^2 \mathrm{d}\Omega, \qquad \dot{\bar{\varepsilon}}^* = \frac{1}{\Omega}\int_\Omega \dot{\bar{\varepsilon}}\,\mathrm{d}\Omega\,, \tag{24}$$

maximum effective strain rate

$$\mathcal{G}_{\dot{\bar{\varepsilon}}_l} = \max_{\Omega}(\dot{\bar{\varepsilon}})\,, \tag{25}$$

overall distortion rate

$$\mathcal{G}_D = \frac{1}{2}\int_{\Omega} \dot{\varepsilon}_{12}\,\mathrm{d}\Omega\,, \tag{26}$$

maximum distortion rate

$$\mathcal{G}_{\dot{\varepsilon}_{12}} = \max_{\Omega}(\dot{\varepsilon}_{12})\,. \tag{27}$$

The corresponding optimized die profiles are shown in Figs. 3 to 5.

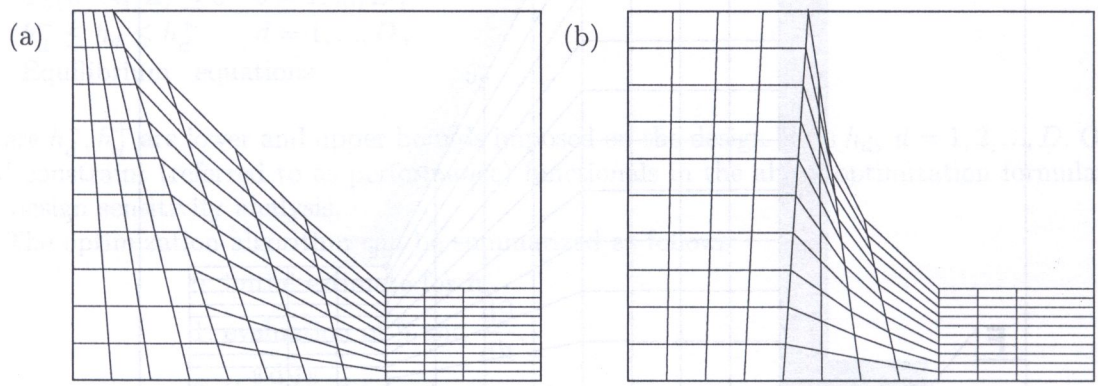

Fig. 3. Optimal shape – Minimization criteria: (a) energy rate, (b) maximum local energy rate

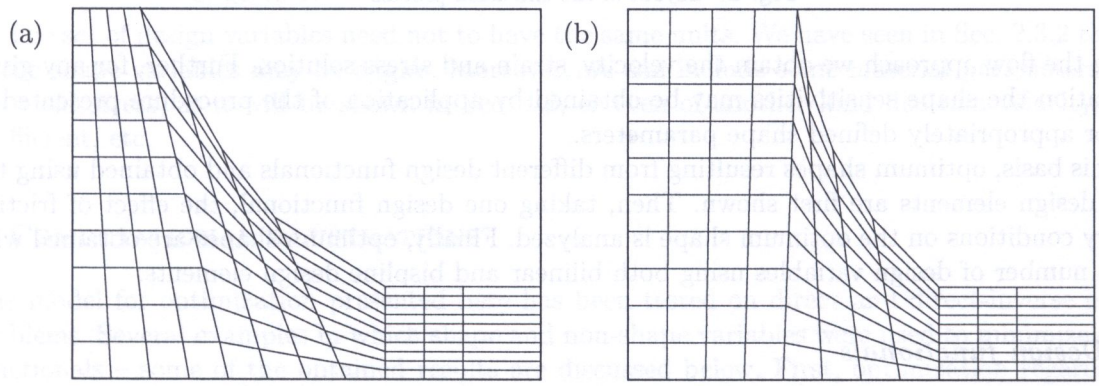

Fig. 4. Optimal shape – Minimization criteria: (a) averaged effective strain rate deviation, (b) maximum local effective strain rate

Since, within bilinear design elements, the profile to be optimized is defined by a polygonal line joining the design points, we impose restrictions on the coordinates of every two neighbouring design points in order to avoid unrealistic situations which may appear during the optimization iterations and disturb the convergence of the optimization process. Numbering the design nodes from left to right and taking only the horizontal components X_1^α as design variables, we should have $X_1^{\alpha+1} \geq X_1^\alpha$.

Table 1 shows the reduction in the value of all the considered functionals achieved after optimization with respect to the x coordinate of the four nodes defining the die profile (A-D, cf. Fig. 2).

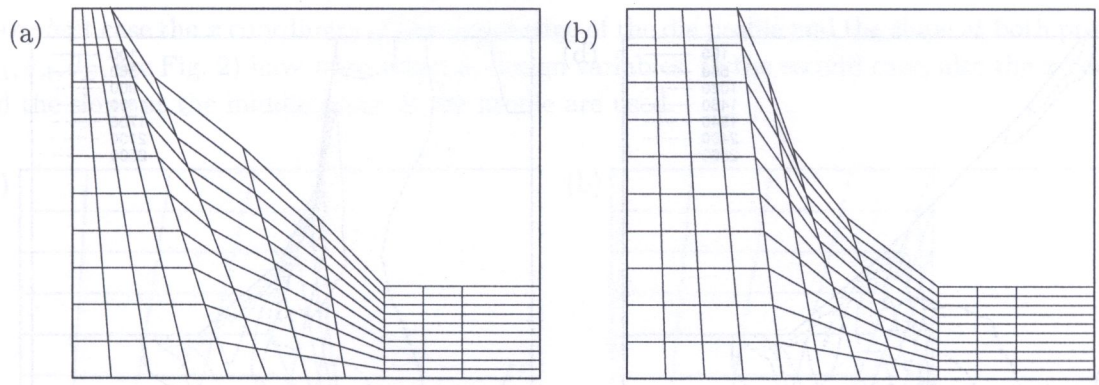

Fig. 5. Optimal shape – Minimization criteria: (a) overall distortion rate, (b) maximum local distortion rate

Table 1. Initial and optimal values of the design functionals

Functional	$\mathcal{G}_E$	$\mathcal{G}_e$	$\mathcal{G}_{D\dot{\bar{\varepsilon}}}$	$\mathcal{G}_{\dot{\bar{\varepsilon}}_l}$	$\mathcal{G}_D$	$\mathcal{G}_{\dot{\varepsilon}_{12}}$
Initial value	0.8658E+5	0.3684E+6	4.802	6.8844	7.119	5.068
Optimal value	0.7922E+5	0.2686E+6	2.913	5.3424	6.358	3.997

We can see in Figs. 3 to 5 two different families of optimal shapes corresponding to either local or global functional character.

For the specific case of the overall deformation energy (Fig. 3) the global functional presents a slightly curved optimal die profile while the corresponding local criterion (i.e. minimization of the maximum local plastic deformation energy rate) exhibits a strongly concave profile. It is interesting to notice, however, that both give approximately the same angle between the die and the material outlet, which is the most critical zone, for its strain rate and stress concentration.

Comparative plots of the energy rate are shown for the initial (Fig. 6), and modified (Fig. 7(a) and (b)) configurations, optimized with respect to both globally and locally defined cost functionals. It can be seen that the last plot shows visible differences with respect to the original and the globally-optimized ones, which suggests that the minimum for both the criteria (local and global) are very different. On the other hand, the isocurves of the energy rate have a similar pattern in both the initial and the global-optimized configurations: in the latter, smoother energy gradients and the deformation zone more spread throughout the domain, can be seen.

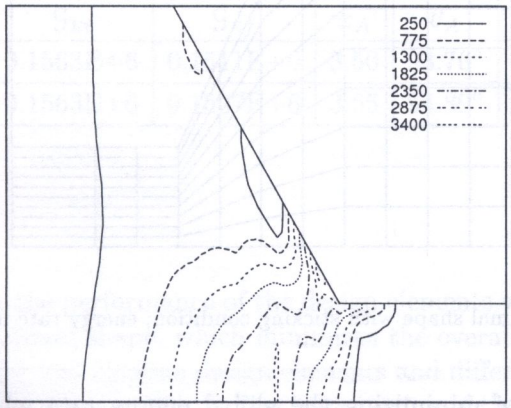

Fig. 6. Energy rate isocurves for the initial die

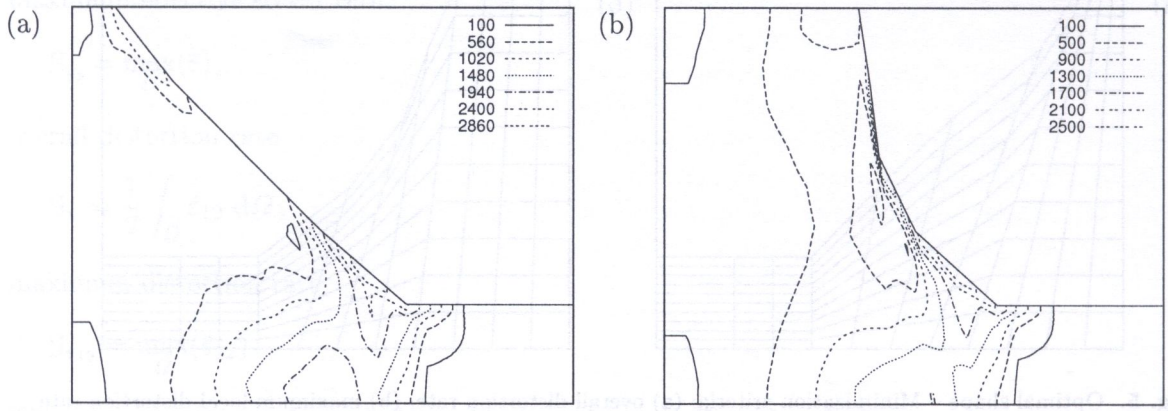

Fig. 7. Energy rate isocurves for (a) global- and (b) local-energy-rate optimized die

4.1.2. Effect of boundary conditions

The optimal solution also depends strongly on the boundary conditions. In contrast with the solutions already shown, where no friction conditions have been assumed, Fig. 8 shows the optimal solution with respect to the deformation energy rate criterion (22) for a problem modeled with sticking (i.e. no slip) condition. Now the design variable is the y-coordinate of the central node of the die profile. A different optimal shape is obtained, as compared to the case with frictionless boundaries. But, as before, the die shape is mainly characterized by the die angle at the outlet, which now is much larger. Besides, a much less significant reduction of the cost functional has been achieved: from $\mathcal{G}_{E0} = 0.1552E + 6$ down to $\mathcal{G}_{Ef} = 0.1530E + 6$. This behaviour results from the effect of the boundary conditions: a zone is developed where the material remains attached to the boundary thus, roughly speaking, design variations only change the size of this zone, which however has a small contribution to the energy integral.

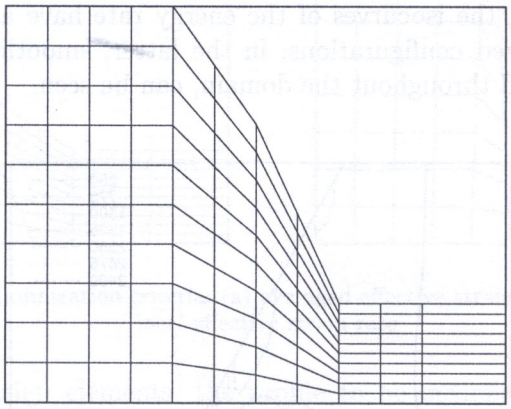

Fig. 8. Optimal shape with sticking condition; energy rate minimization

Next, the same problem of minimizing the global energy rate when the sticking condition is assumed is solved using the bispline design elements presented in Sec. 2.3.2. Figure 9 shows the optimal shapes of the extrusion die for such boundary condition assumed along the whole boundary.

In the first case the x coordinate of the upper edge of the die profile and the slope at both profile ends (x_A, θ_A, θ_E, see Fig. 2) have been taken as design variables. In the second case, also the x-coordinate and the slope at the middle point of the profile are used.

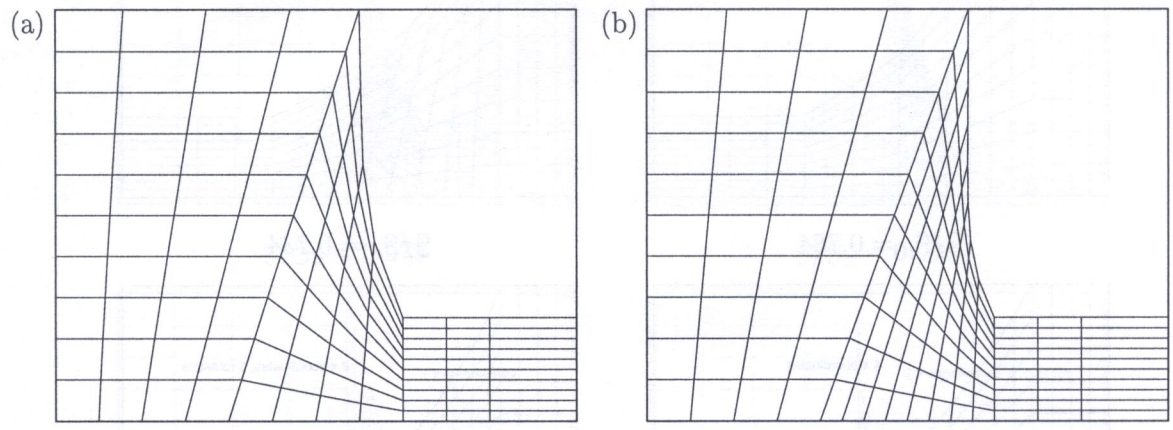

Fig. 9. Optimal shape – (a) three and (b) five design variables

We can see that the solution with more design variables approximates better a "square" profile at the die corner, with a transition at the die exit. The angle at the die exit is very similar in both cases, as results from Table 2. The solution is in agreement with the empirically optimized dies for such boundary conditions, where the dead zone forms a kind of internal optimal die. However, we can see also from Table 2 that the cost functional is roughly the same for both solutions, which means that it may not be worth to reach an exact optimum if this involves some technological difficulties. Moreover, the same example using only one degree of freedom (the y-coordinate of the middle point, y_C) already shown, see Fig. 8, solved using bilinear design elements, yields a functional value of $\mathcal{G}_{Ef}$=0.153E+6 with, again, a similar die angle at the exit [29], which shows to be the most critical variable for optimization. In the present discussion, however, it should be noticed that the constitutive model used here fails to model the real material behaviour at the shear band that develops within the dead-zone formation. The extrusion force drops when the dead zone arises, as it comes out from experiments, but this fact is not reflected within this model.

Table 2. Initial and optimal values of the design functionals and of the design variables

	$\mathcal{G}_{Ei}$	$\mathcal{G}_{Ef}$	x_A	θ_A	θ_E
D=3	0.1563E+6	0.1511E+6	3.50	93.76°	121.38°
D=5	0.1563E+6	0.1507E+6	3.65	94.89°	122.05°

4.1.3. Design elements

Finally, to further investigate the performance of the design elements with different design variables, the problem of finding the optimal shape, which minimizes the overall deformation energy rate has been solved using both bilinear and bispline design elements and different sets of design parameters. Again, the initial shape is that given in Fig. 2. The initial value of the design functional is given as reference to be compared with the optimized results. The optimal shapes arrived at are shown in Figs. 10 and 11 for the frictionless and sticking-condition cases, respectively. Whenever only spatial

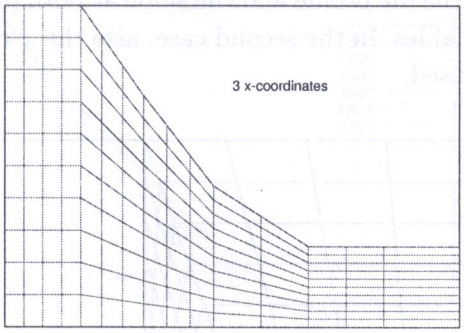

$\mathcal{G}/\mathcal{G}_o = 0.784$

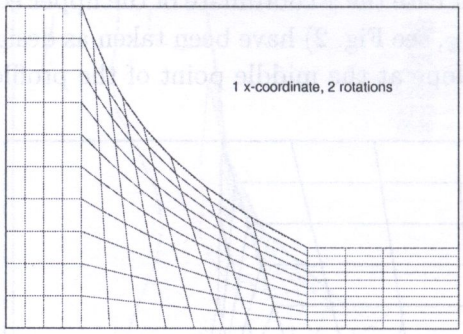

$\mathcal{G}/\mathcal{G}_o = 0.734$

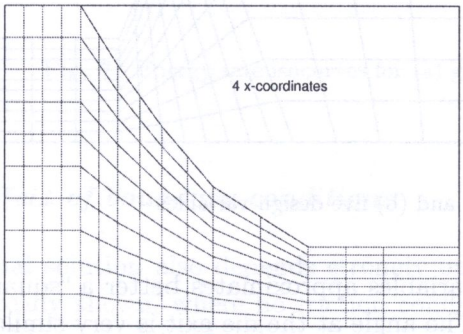

$\mathcal{G}/\mathcal{G}_o = 0.780$

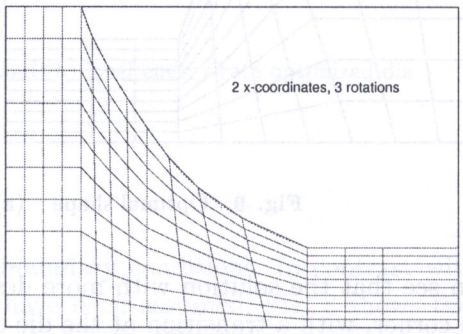

$\mathcal{G}/\mathcal{G}_o = 0.7054$

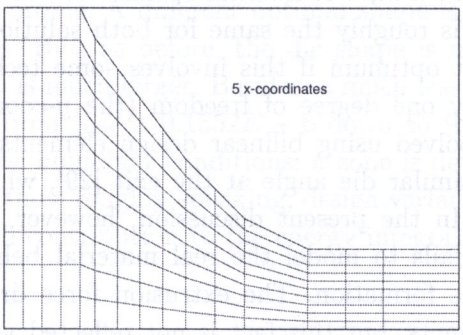

$\mathcal{G}/\mathcal{G}_o = 0.748$

Fig. 10. Shape optimization for frictionless boundary. Bilinear and bispline elements

coordinates are considered as design variables (i.e. no rotation angles of the design border at the design node), the bispline elements reduce to bilinear. All the results are summarized in Table 3. It can be seen that the relative reduction in the cost functional is better noticeable in the frictionless case than with sticking-condition boundaries. As said earlier, this behaviour obeys to a physical fact. From the numerical side, the bispline elements show to be very effective: whenever the cost functional value may be lowered by design, for the frictionless case, with the same number of degrees of freedom (that is, design parameters), a more important reduction in the design functional is obtained. The case with sticking friction shows, as before, a non-significant gain. As already argued, in such case a dead zone develops with which the material itself finds its own optimal internal die, since our numerical solution minimizes the same energy functional. Besides, it is even noticed that increasing the number of design parameters the optimized functional is higher than with less design parameters. This fact suggests the presence of local minima which are probably connected with the material model in the $\dot{\bar{\varepsilon}} \to 0$ limit, in which, a cutoff value is applied for the viscosity μ [8, 28].

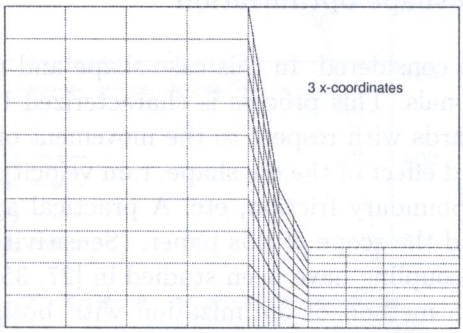

$\mathcal{G}/\mathcal{G}_o = 0.973$

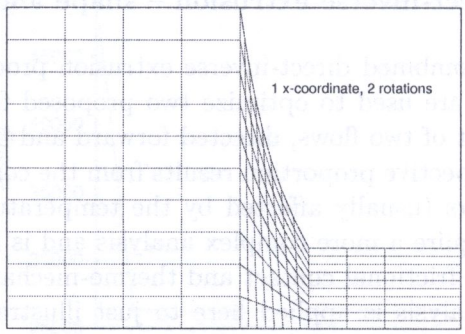

$\mathcal{G}/\mathcal{G}_o = 0.976$

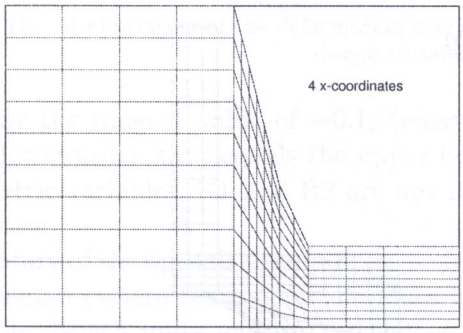

$\mathcal{G}/\mathcal{G}_o = 0.976$

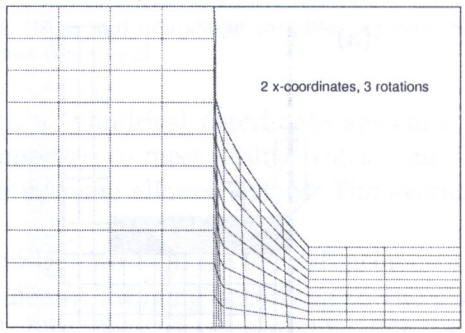

$\mathcal{G}/\mathcal{G}_o = 0.976$

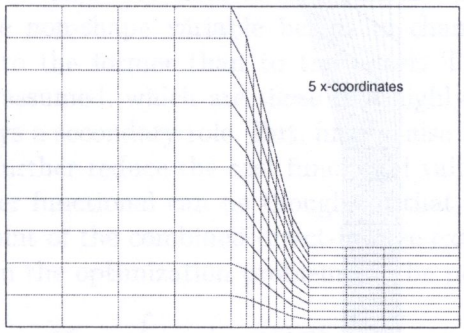

$\mathcal{G}/\mathcal{G}_o = 0.976$

Fig. 11. Shape optimization for sticking condition. Bilinear and bispline elements

Table 3. Initial and optimal values of the design functionals

	Frictionless boundaries		Sticking friction	
Init. Value:	$\mathcal{G}_o = 86343$	$\mathcal{G}/\mathcal{G}_o$	$\mathcal{G}_o = 156282$	$\mathcal{G}/\mathcal{G}_o$
bilinear elements:				
$3X + 0\theta$	$\mathcal{G} = 67667$	0.784	$\mathcal{G} = 152120$	0.973
$4X + 0\theta$	$\mathcal{G} = 67388$	0.780	$\mathcal{G} = 152461$	0.976
$5X + 0\theta$	$\mathcal{G} = 64618$	0.748	$\mathcal{G} = 152522$	0.976
bispline elements:				
$1X + 2\theta$	$\mathcal{G} = 63408$	0.734	$\mathcal{G} = 152609$	0.976
$2X + 3\theta$	$\mathcal{G} = 60903$	0.705	$\mathcal{G} = 152575$	0.976

4.2. Direct-inverse extrusion – shape and non-shape optimization

Next, a combined direct-inverse extrusion process is considered. In this case shape and non-shape variables are used to optimize two proposed functionals. This process is characterized by the development of two flows, directed forward and backwards with respect to the movement of the ram. Their respective proportion results from the combined effect of the die shape, ram velocity, material parameters (usually affected by the temperature), boundary friction, etc. A practical application would require a more complex analysis and is beyond the scope of this paper. (Sensitivity analysis regarding frictional contact and thermo-mechanical coupling have been studied in [27, 35]). A simplified analysis is applied here to just illustrate the method of optimization with both types of variables.

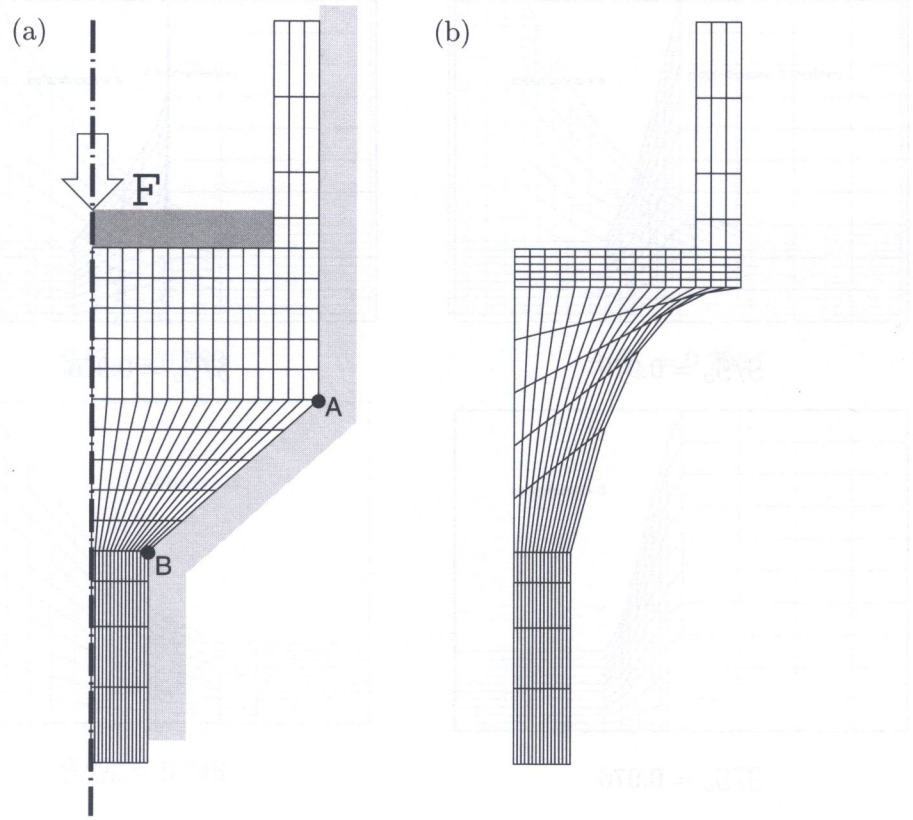

Fig. 12. Direct-inverse extrusion: a) layout and initial shape, b) final shape after minimization of the deformation energy w.r.t. shape and non-shape variables

Figure 12(a) presents a scheme of the process. An axisymmetric billet is placed on a die in which, by the action of a mandrel part of the metal is extruded downwards, but since there is some space between the mandrel and the die, a counterflow is formed upwards. The process is considered in a quasi-steady state. The diameters at both outlets are considered fixed, but the actual shape of the die is subject to design. To this aim, the vertical coordinate of point A (X1 in Fig. 13 and 15), and the die angle at points A and B (θ_1 and θ_2 in Fig. 13 and 15) are subject to design. The shape sensitivity analysis is performed with the aid of the design elements with bispline interpolation. Additionally, the material yield stress σ_0 (cf. Eq. (3)) is also taken as a design variable. The rate of energy insumed in the process of plastic deformation is taken as the first cost functional to be minimized, Eq. (22). The final shape arrived at shows that point A (X1) has moved upward taking a die-profile angle as large as possible with respect to the overall flow direction, which is

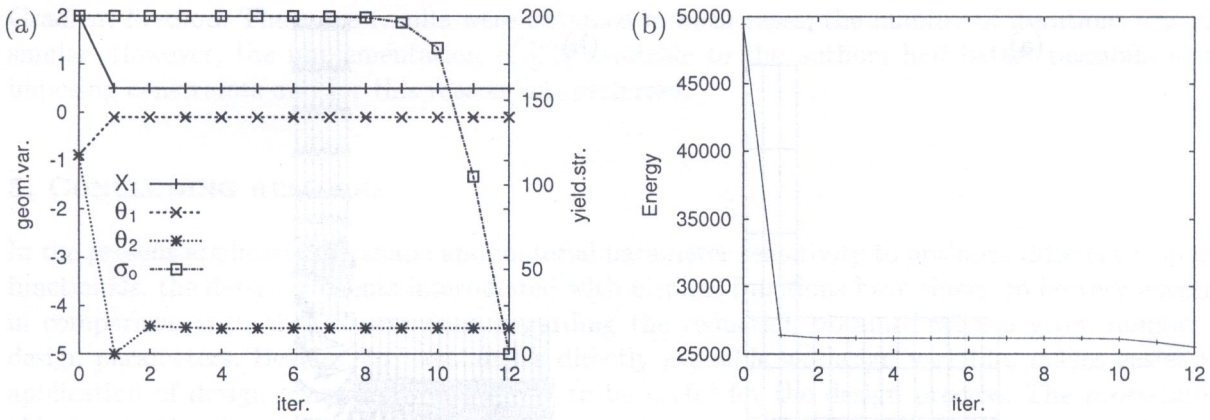

Fig. 13. Minimization of the deformation energy w.r.t. shape and non-shape variables: a) evolution of design variables, b) cost functional

reflected by the tangent value of -0.1, (measured in a cylindrical coordinate system r, z, with z directed downwards), that equals the upper bound imposed to meet desing restrictions. The other two geometric variables, R1 and R2 are not at their extreme allowed values. The overall shape is quite concave.

The history of the optimization process is shown in Fig. 13(a). On the left axis geometric variables are represented (where the numerical values have different meaning according to the character of the variable: length units -cm- or tangent of angle). The three shape variables fall very close to their optimal value already in the second design iteration. In this first period the cost functional also takes a value very close to the optimum. Small changes are still applied to the shape variables before the non-shape variable begins to change, because the response functional is much more sensitive to the former than to the latter. This is especially true regarding the set of material variables assumed, which are those of a highly rate-sensitive material, from which the static yield stress plays a secondary role. But, finally, also the yield stress falls to its minimum allowed value in order to further reduce the cost functional value.

Another functional can be thought of that may show useful to design processes of this type. If the keypoint of the combined direct-inverse extrusion is to keep a desired proportion between both flows, then the optimization problem can be posed as that of minimizing the functional

$$\mathcal{G} = \mathcal{G}_d - f\mathcal{G}_i = \int_{\partial\Omega_d} \mathbf{v}\cdot\mathbf{n}\,\mathrm{d}(\partial\Omega) - f\int_{\partial\Omega_i} \mathbf{v}\cdot\mathbf{n}\,\mathrm{d}(\partial\Omega) \tag{28}$$

where $\partial\Omega_d$ and $\partial\Omega_i$ are the outlets for the direct and inverse flows, respectively, and f is a real number that determinates the required proportion between both flows. Here $f = 1$ has been assumed, meaning the condition that the forward and backward flows should be equal. Additional restrictions that would obey e.g. to some constructive criteria are imposed as usual. The final shape after optimization is shown in Fig. 14(a). Using again the same variables as before, minimization of the above functional yields a practically straight die profile with the die corner displaced down to it design bound. Fig. 14(b) presents the velocity field. After the uniform velocity imposed by the ram, a flow bifurcation is observed. This zone begins right after the right corner of the ram. The particles flowing downwards (direct flow) show a sensible increase of the velocity module, fulfilling the incompressibility condition. Both flows become practically uniform right after leaving the die. The optimization process also in this case leads to a design close to the optimum after two design iterations. This can be clearly appreciated in Fig. 15(a) and (b), where the values the design parameters take and that of the response functional are shown. It is also evident that the actual value of the yield stress does not affect the relative flows, thus its value remains constant.

The computations presented in this Section were carried out using Schittkowski's algorithm [32]. The case shown in Fig. 8 (like many others not presented here) was also solved using the Conjugate

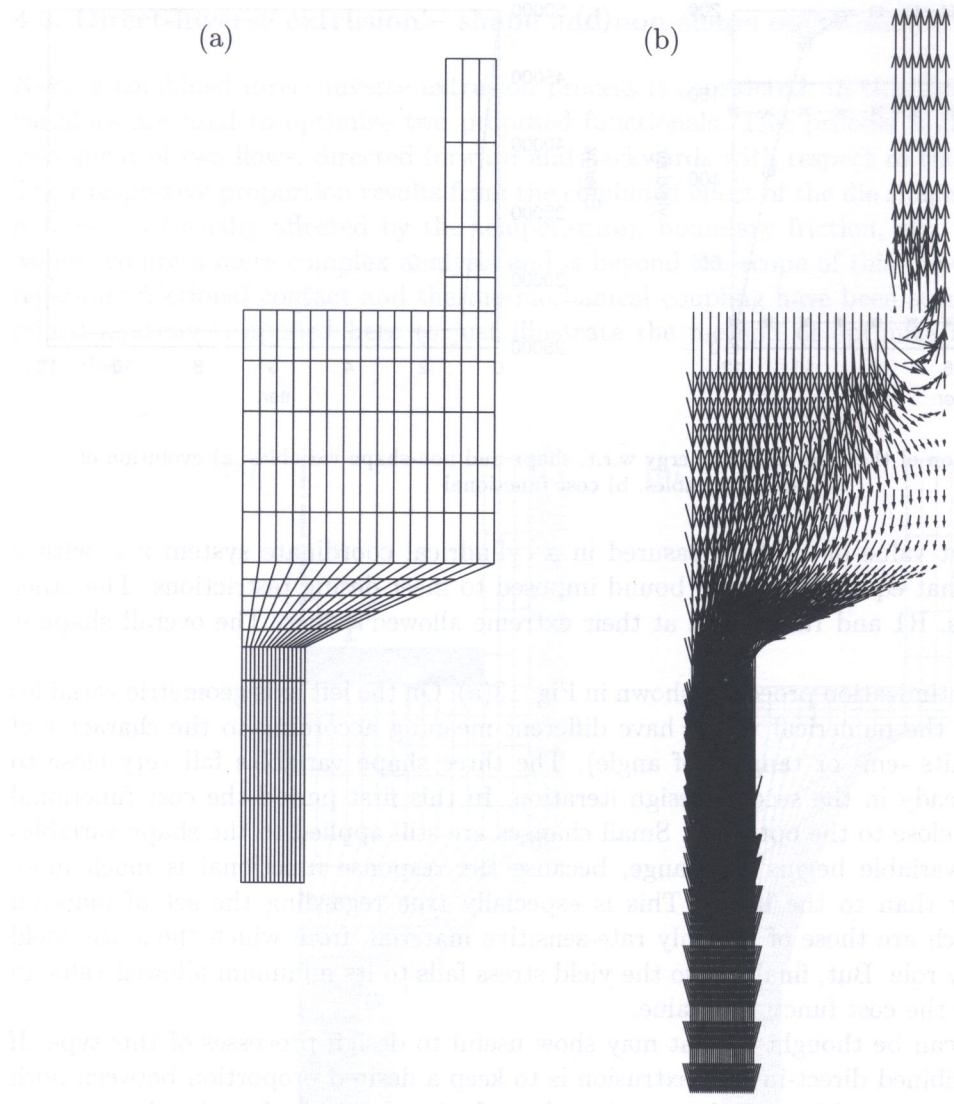

Fig. 14. Minimization of the difference direct-inverse flow w.r.t. shape and non-shape variables: (a) final mesh, (b) velocity field

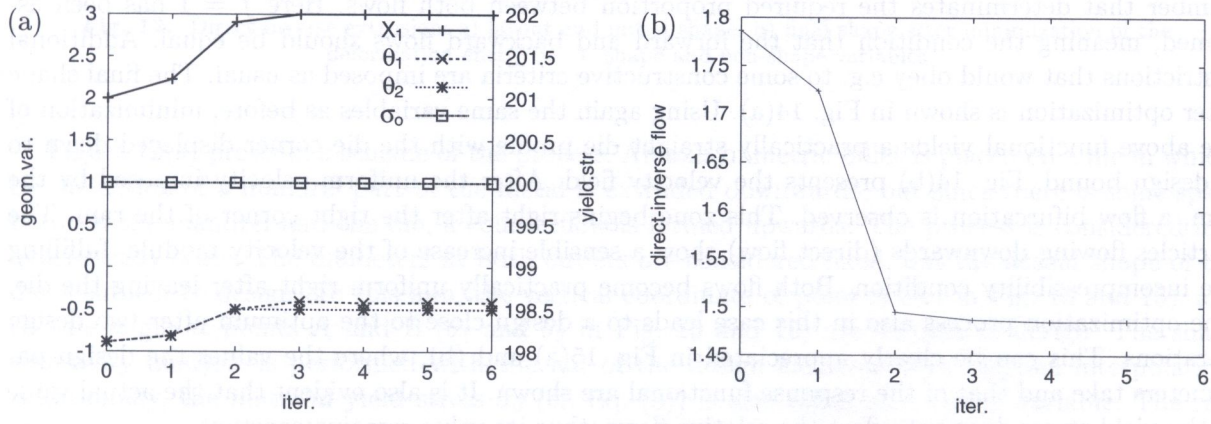

Fig. 15. Minimization of the difference direct-inverse flow w.r.t. shape and non-shape variables: a) evolution of design variables, b) cost functional

Gradient Method. The same results were obtained in both cases; the number of iterations was also similar. However, the implementation of [32] available to the authors had better possibilities for imposing constraints and for this reason was preferred.

5. Concluding remarks

In the present application of shape and material parameter sensitivity to optimize different response functionals, the design elements interpolated with bispline functions have shown to be very effective in comparison with the bilinear ones, regarding the reduction obtained with a given number of design parameters. Besides, to have angles directly available as design variables makes easier the application of design constraints and shows to be useful for the design process. The procedure is able to combine in a same optimization process shape and other type of design parameters and shows a certain degree of generality for its application to other geometries and processes.

References

[1] Z. Mróz, M. P. Kamat, R. H. Plant. Sensitivity analysis and optimal design of nonlinear beams and plates. *J. Struct. Mech.*, **13**: 245–266, 1985.

[2] Z. Mróz. Variational methods in sensitivity analysis and optimal design. *Eur. J. Mech. A/Solids*, **13**: 115–147, 1994.

[3] D. A. Tortorelli, J. A. Tomasko, T. E. Morthland, J. A. Dantzig. Optimum design of nonlinear parabolic systems. part ii: Variable spatial domain with applications to casting optimization. *Comput. Meth. Appl. Mech. Engrg.*, **113**: 157–172, 1994.

[4] J. Kusiak. *Optimization techniques in computer simulation of metal forming processes* (in Polish). Wydawnictwo AGH, Kraków, 1995.

[5] J. Kusiak, E. G. Thompson. Optimization techniques for extrusion die shape design. In E. G. Thompson, R. D. Wood, O. C. Zienkiewicz, A. Samuelsson, editors, NUMIFORM'89, *Numerical Methods in Industrial Forming Processes*, pages 569–574. Balkema, 1989.

[6] C. S. Han, R. V. Grandhi, R. Srinivasan. Optimum design of forging die shapes using nonlinear finite element analysis. *AIAA J.*, **31**: 774–781, 1993.

[7] M. S. Joun, S. M. Hwang. Die shape optimal design in three-dimensional shape metal extrusion by the finite element method. *Int. J. Numer. Methods Eng.*, **41**: 311–335, 1998.

[8] H. J. Antúnez, M. Kleiber. Sensitivity of forming processes to shape parameters. *Comput. Meth. Appl. Mech. Engrg.*, **137**: 189–206, 1996.

[9] S-Y. Wang, Y. Sun, R. H. Gallagher. Sensitivity analysis in shape optimization of continuum structures. *Comput. Struct.*, **20**(5): 855–867, 1985.

[10] R. J. Yang, M. E. Botkin. Accuracy of the domain material derivative approach to shape design sensitivities. *AIAA J.*, **25**(12): 1606–1610, 1987.

[11] J. S. Arora. An exposition of the material derivative approach for structural shape sensitivity analysis. *Comput. Meth. Appl. Mech. Engrg.*, **105**: 41–62, 1993.

[12] J. P. Zolesio. The material derivative (or speed) method for shape optimization. In E. J. Haug and J. Cea, editors, *Optimization of Distributed Parameter Structures*. Sijthoff & Noordhoff, 1981.

[13] L. Fourment, T. Balan, J. Chenot. Shape optimization for the forging process. In D. R. J. Owen, E. Oñate, and E. Hinton, editors, *Computational Plasticity, Proc. COMPLAS IV*, pages 1369–1381. Barcelona, Pineridge Press, 1995.

[14] L. Fourment, T. Balan, J. L. Chenot. Optimal design for non-steady-state metal forming processes–ii. application of shape optimization in forging. *Int. J. Numer. Methods Eng.*, **39**(1): 51–65, 1996.

[15] L. Fourment, J. L. Chenot. Optimal design for non-steady-state metal forming processes–i. shape optimization method. *Int. J. Numer. Methods Eng.*, **39**(1): 33–50, 1996.

[16] S. M. Byon, S. M. Hwang. Process optimal design in non-isothermal, steady-state metal forming by the finite element method. *Int. J. Numer. Methods Eng.*, **46**(7): 1075–1100, 1999.

[17] S. H. Chung, S. M. Hwang. Optimal process design in non-isothermal, non-steady metal forming by the finite element method. *Int. J. Numer. Methods Eng.*, **42**(8): 1343–1390, 1998.

[18] S. M. Byon, S. M. Hwang. Fem-based process optimal design in steady-state metal forming considering strain-hardening. *Comput. Struct.*, **79**(14): 1363–1375, 2001.

[19] I. Doltsinis, T. Rodic. Process design and sensitivity analysis in metal forming. *Int. J. Numer. Methods Eng.*, **45**(6): 661–692, 1999.

[20] Y.H. Park, K.K. Choi. Shape design sensitivity analysis of nonlinear 2-d solids with elasto-plastic material. *Struct. Optimization*, **18**(4): 236–246, 1999.

[21] D. Balagangadhar, D.A. Tortorelli. Design of large-deformation steady elastoplastic manufacturing processes. part ii: sensitivity analysis and optimization. *Int. J. Numer. Methods Eng.*, **49**: 933–950, 2000.

[22] Z.H. Huang, M. Lucas, M.J. Adams. Modelling wall boundary conditions in an elasto-viscoplastic material forming process. *J. Mater. Process. Tech.*, **107**(1-3): 267–275, 2000.

[23] N.H. Kim, K.K. Adams, J.S. Chen. Meshless shape design sensitivity analysis and optimization for contact problem with friction. *Comput. Mech.*, **25**(2-3): 157–168, 2000.

[24] A. Srikanth, N.B. Zabaras. Shape optimization and preform design in metal forming processes. *Comput. Meth. Appl. Mech. Engrg.*, **190**: 1859–1901, 2000.

[25] N.B. Zabaras, Y.G. Bao, A. Srikanth. A continuum lagrangian sensitivity analysis for metal forming processes with applications to die design problems. *Int. j. numer. methods eng.*, **48**(5): 679–720, 2000.

[26] H.J. Antúnez, M. Kleiber. Parameter sensitivity of metal forming processes. *Comput. Assisted Mech. Eng. Sci.*, **3**: 263–282, 1996.

[27] H.J. Antúnez, M. Kleiber. Sensitivity analysis of metal forming processes involving frictional contact in steady state. *J. Mater. Proc. Technology*, **60**: 485–491, 1996.

[28] M. Kleiber, H.J. Antúnez, T.D. Hien, P. Kowalczyk. *Parameter Sensitivity in Nonlinear Mechanics.* Wiley, Chichester, 1997.

[29] H.J. Antúnez, M. Kleiber, W. Sosnowski. Shape and non-shape sensitivity and optimization of metal forming processes. In E. Oñate, D.R.J. Owen, and E. Hinton, editors, *Computational Plasticity, Proc. COMPLAS VI*, pages 783–791. Barcelona, Pineridge Press, 1997.

[30] M. Kleiber. Shape and non-shape sensitivity analysis for problems with any material and kinematic nonlinearity. *Comput. Meth. Appl. Mech. Engrg.*, **108**: 73–97, 1993.

[31] R. Fletcher C.M. Reeves. Function minimization by conjugate gradients. *Computer Journal*, **7**: 149–154, 1964.

[32] K. Schittkowski. `NLPQL`: a fortran subroutine solving constrained nonlinear programming problems. *Annals of Operations Research*, **5**: 485–500, 1986.

[33] J.S. Arora, T.H. Lee, J.B. Cardoso. Structural shape sensitivity analysis: relationship between material derivative and control volume approaches. *AIAA J.*, **30**: 1638–1648, 1992.

[34] J.S. Badrinaraganan, N.B. Zabaras. A sensitivity analysis for the optimal design for metal-forming processes. *Comput. Meth. Appl. Mech. Engrg.*, **129**: 319–348, 1996.

[35] H.J. Antúnez. Thermo-mechanical modelling and sensitivity analysis for metal-forming operations. *Comput. Meth. Appl. Mech. Engrg.*, **161**: 113–125, 1998.

[36] H.J. Antúnez, M. Kowalczyk. Sensitivity based optimal design of metal forming processes accounting for shape and non-shape variables. In M. Pietrzyk, Z. Mitura, J. Kaczmar, editors, Proc. *The 5^{th} Internatonal ESAFORM Conference on Material Forming*, pages 23–26, Kraków, Publishing House "Akapit", 2002.